Fuel 362 (2024) 130857

Contents lists available at ScienceDirect

Fuel

journal homepage: www.elsevier.com/locate/fuel

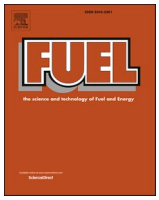

Full Length Article

The pyrolysis of 4,4,8,10-tetramethyl decalin and the influence of molecular structures on oil thermal cracking: A ReaxFF molecular dynamics simulation and DFT study

Haochen Chen [a], Meijun Li [a,b,*], Xiaoqiang Liu [b], Qiuya Han [a], Wenke Li [c], Siyuan Zhang [a]

[a] National Key Laboratory of Petroleum Resources and Engineering, China University of Petroleum (Beijing), Beijing 102249, China
[b] College of Petroleum, China University of Petroleum (Beijing) at Karamay, Xinjiang 834000, China
[c] College of Chemistry and Environmental Engineering, Sichuan University of Science and Engineering, Zigong 643000, China

ARTICLE INFO

Keywords:
Reactive molecular dynamics simulation
Density functional theory
4,4,8,10-Tetramethyl decalin
Pyrolysis
Kinetics

ABSTRACT

The molecular structure of different hydrocarbons in crude oil has a significant effect on the thermal cracking mechanism. This study delves into the thermal cracking mechanism, pyrolysis process, and kinetics of 4,4,8,10-tetramethyl decalin (a representative bicyclic sesquiterpane in crude oil) using reactive molecular dynamics simulation (ReaxFF–MD) at the temperature range from 2000 K to 3000 K. Interestingly, the major intermediate products from thermal pyrolysis simulation align closely with the main ion fragments in the mass spectrometry of 4,4,8,10-tetramethyl decalin. The results can be directly used to analyze the pyrolysis mechanism. It reveals five reaction pathways implicated in the initial pyrolysis of 4,4,8,10-tetramethyl decalin: three demethylation reactions (more likely to occur) and two ring-opening reactions. By employing first-order kinetic analysis based on ReaxFF–MD simulations within the temperature range of 2000 K to 3000 K, the apparent activation energies for 4,4,8,10-tetramethyl decalin are calculated and compared with our prior simulation results for *n*-tetradecane. The initial pyrolysis of 4,4,8,10-tetramethyl decalin predominantly entails the cleavage of C–C bonds in both branched chain and carbon ring systems, resulting in the generation of methyl and high molecular weight ring-structured radicals. Conversely, the initial pyrolysis of *n*-tetradecane yields low molecular weight straight–chain radicals by cleaving C–C bonds except for the terminal position. This implies that the bicyclic sesquiterpane 4,4,8,10-tetramethyl decalin serves as the favorable precursor for producing methane (CH_4) and liquid hydrocarbons (C_6–C_{13}) during the primary formation stage of light oil. With an equivalent number of carbon atoms, *n*-tetradecane serves as the preferred precursor for generating wet gases (C_2–C_5) at the initial formation stage of wet gases. The insights derived from the ReaxFF–MD simulation offer valuable perspectives for comprehending the process of thermal cracking in crude oil under geological conditions.

1. Introduction

4,4,8,10-Tetramethyl decalin is a representative bicyclic sesquiterpane with a decahydronaphthalene skeleton substituted by C_4, C_8 and C_{10} alkyl side chains [1–5]. 4,4,8,10-tetramethyl decalin (C_{14}) with the drimane type (C_{15}–C_{16}) skeleton is widely distributed in crude oil and sediments. Alexander et al. [5] suggest that bicyclic sesquiterpanes are the products formed by the degradation of bacterial hopane at the early stage of diagenesis. In the later diagenetic process, a variety of isomers were formed by defunctionalization and rearrangement. The C_{14}–C_{16} drimane series is generally formed by bacteria and other microbes. And the bicyclic sesquiterpanes have been employed to differentiate the organic matter input from various sedimentary environments and classed as an organic source indicator that widely justifies the applications of relative proportions of the C_{14}–C_{16} bicyclanes in oil-source correlation [6–8]. C_{15}-C_{16} bicyclic sesquiterpanes, namely, 8β(H)-drimane, 8β(H)-homodrimane, and 8α(H)-homodrimane, are commonly used to indicate the maturity of samples in the immature-low-maturity stage due to their relatively high sensitivity to temperature changes. Yan et al. [1], Luo et al. [2], and Xia et al. [3] reported the ratios 8β(H)-drimane/8β(H)-homodrimane, 8β(H)-homodrimane/8α(H)-homodrimane, and 8β(H)-drimane/8α(H)-homodrimane increased with the degree of thermal evolution before the temperature turning point. Compared with C_{15} and C_{16}, abandoned C_{14} bicyclic sesquiterpanes

* Corresponding author.
E-mail address: meijunli@cup.edu.cn (M. Li).

https://doi.org/10.1016/j.fuel.2024.130857
Received 12 August 2023; Received in revised form 4 November 2023; Accepted 1 January 2024

detected in crude oil have rarely been studied for their thermochemical property.

Pyrolysis experimentation is an effective technology to quantitatively investigate the thermal evolution of hydrocarbons in crude oil. The principle is that temperature and time exert complementary effects on the hydrocarbon generation process within sedimentary layers [9]. However, only brief descriptions of product characteristics were provided. ReaxFF–MD simulation [10] offers an insightful analysis of intricate chemical reactions, encompassing the examination of intermediates. This analysis was conducted within a timescale ranging from femtoseconds to picoseconds. Numerous investigations of the thermal decomposition phenomenon of diverse components within fossil fuels and petroleum have been provided by ReaxFF–MD over the past decades [11–16].

For instance, Salmon et al. (2008) [17] show that the initial pyrolysis mechanism of algous biopolymer is the cleavage of the C–O bond in the ester group, accompanied by the formation of isoprenoid structure by the cleavage of C–C. In addition, ReaxFF–MD simulation was performed to study the pyrolysis process of defunctionalization, depolymerization, and rearrangement of coal structures observed in the experimental studies [18–20]. The scission of C–C bonds is the main way to generate gaseous hydrocarbons during the thermal evolution of coal. On the other hand, the pyrolysis chemistries of some straight-chain alkanes, such as *n*-heptane (C_7H_{16}) [11], *n*-dodecane ($C_{12}H_{26}$) [21], *n*-tetradecane ($C_{14}H_{30}$) [16], *n*-hexadecane ($C_{16}H_{34}$) [22], and *n*-eicosane ($C_{20}H_{42}$) [23], have also been simulated by ReaxFF molecular dynamics. The results indicate that the homolytic fission of C–C bonds plays a dominant role in the whole pyrolysis process of *n*-alkanes in contrast to dehydrogenation reactions. For branched-chain alkanes, Xin et al. [13]and Tian et al. [24,25] found the pyrolysis of branched hydrocarbons occurs earlier than that of straight-chain hydrocarbons. The pyrolysis rates of paraffin gradually increase with the increase of chain length with a similar molecular structure. For cycloalkane, the dissociation of substituents on the ring and the cleavage of adjacent C–C bonds on the ring (ring-opening reaction) are the main initial decomposition mechanisms of naphthenic hydrocarbons [12,15,26–30]. Therefore, the type and carbon number of substituents on rings and the number of carbocyclic rings have a significant effect on the position of bond cleavage and the key products of initial pyrolysis channels. Additionally, it was found that the order of thermal decomposition of various petroleum compounds with the same number of carbon atoms is as follows: cycloalkane > branched-chain alkanes > straight-chain alkane [13]. Many studies have used ReaxFF–MD to explore the reaction mechanisms of petroleum components, however, the effects of single-component reaction mechanisms on the formation and preservation of petroleum have not been discussed in geological conditions.

In order to investigate the effects of different pyrolysis mechanisms of normal alkane and biomarkers on the cracking of crude oil, a series of MD simulations of 4,4,8,10-tetramethyl decalin is performed in this study. After that, comparing the simulation results of 4,4,8,10-tetramethyl decalin with *n*-tetradecane, excluding the influence of the number of carbon atoms, the specific effects of bicyclic sesquiterpanes and *n*-alkanes with different molecular structures on the cracking of crude oil into natural gas were discussed deeply. The apparent activation energy of 4,4,8,10-tetramethyl decalin pyrolysis was also calculated to test the accuracy and reliability of the simulation. This study would be expected to afford a reasonable reference for the research of the C_{14} bicyclic sesquiterpene and the exploration of ultradeep-buried petroleum reservoirs under high formation temperatures.

2. Computational methods

2.1. The construction of 4,4,8,10-tetramethyl decalin molecular models

According to the results of gas chromatography-mass spectrometry (GC–MS) analyses of the oil sample from Well NE-3 in the eastern Baiyun Sag (Pearl River Mouth Basin, South China Sea), the biomarker 4,4,8,10-tetramethyl decalin was identified on mass chromatograms of *m/z* 179 diagnostic fragment and confirmed by the comparison of the mass spectrum with that of literature [1,4,5,39] (Fig. 1).

Similar to our earlier work [16], fifty molecules of 4,4,8,10-tetramethyl decalin were incorporated into a cubic cell using the Amorphous Cell module in Material Studio Software (MS), as shown in Fig. 2. The model contains 2000 atoms, including 700 carbon atoms and 1300 hydrogen atoms, with the chemical formula $C_{700}H_{1300}$. Periodic boundary conditions were applied in all three directions to the initial 4,4,8,10-tetramethyl decalin cell. To prevent molecules from overlapping, the initial density of the cell was set to 0.3 g/cm^3. In order to gain the credible density of the model, the following simulations were performed by the Forcite software package in MS: first, the Geometric Optimization module was employed to achieve an accurate configuration. Subsequently, an Anneal calculation with the constant-pressure, constant-temperature ensemble (NPT) was performed at temperatures ranging from 298.15 to 700 K for 30 cycles to attain the minimum energy configuration of 4,4,8,10-tetramethyl decalin. The lowest energy configuration obtained from the relaxation was considered the initial configuration for a sequence of simulations in the NPT ensemble at 298.15 K and 0.10 MPa for 2000 ps, yielding a reliable density value for the 4,4,8,10-tetramethyl decalin cell.

As shown in Fig. 3(a), the 4,4,8,10-tetramethyl decalin cell reached its equilibrium temperature at 298.15 K, corresponding to the initial temperature. The density of the 4,4,8,10-tetramethyl decalin also reaches equilibrium at 2000 ps, as illustrated in Fig. 3(b). The cell parameters of the 4,4,8,10-tetramethyl decalin cell were determined as follows: a = 25.24 Å, b = 29.19 Å, c = 25.62 Å, $\alpha = 95.89°$, $\beta = 98.12°$ and $\gamma = 102.78°$. It can be confirmed that the model constructed is reliable as the temperature and density have both achieved equilibrium, suggesting that the interactions between the molecules of 4,4,8,10-tetramethyl decalin are stable.

2.2. Reactive molecular dynamics simulation details

The ReaxFF reactive force field is a potent method for molecular simulation that leverages the concept of bond orders to model molecular connectivity, encompassing bonds, angles, and torsions. The extensive applicability of the ReaxFF reactive force field in investigating the thermal pyrolysis mechanisms of various hydrocarbon fuels made it a highly appropriate choice for our study. Using the LAMMPS (Large-scale Atomic/Molecular Massively Parallel Simulator) code with the ReaxFF reaction force field [22], we conducted all molecular dynamics simulations without modifying the ReaxFF CHO-2008 potentials, originally developed by Chenoweth and van Duin [30]. To effectively control pressure and temperature, the NVT (Isochoric-Isothermal) coupled with the Nose-Hoover barostat and thermostat [16,31] was opted in all simulation processes, allowing the maintenance of a constant number of particles (N), volume (V), and temperature (T). The initial system has been optimized in MS mentioned above. Then the system was equilibrated at 300 K for 50 ps with a time step of 0.1 fs. After that, the system was heated to a target temperature of 2000 K–3000 K [16,32,33]. The simulation was performed every 250 K for 500 ps. The heating rate of 10 K/ps was applied to balance computational efficiency with capturing essential dynamics. The bond order cutoff for molecule recognition was set at 0.3. A series of FORTRAN scripts were devised to analyze the decay of 4,4,8,10-tetramethyl decalin and the subsequent formation of smaller molecules, facilitating the investigation of molecular transformations and providing insights into the chemical reactions occurring during the simulations. By employing this comprehensive approach and methodology, valuable insights into the high-temperature behavior of 4,4,8,10-tetramethyl decalin were aimed to be gained, and advancements in our understanding of the intricate chemical reactions involved in pyrolysis were pursued.

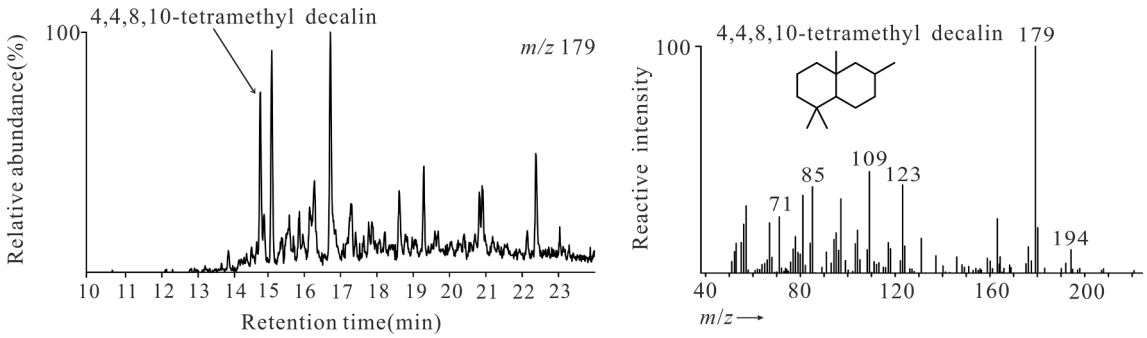

Fig. 1. Identification of 4,4,8,10-tetramethyl decalin in mass chromatogram (*m/z* 179) and mass spectra of 4,4,8,10-tetramethyl decalin from full-scan GC–MS analysis of an oil sample from the eastern Baiyun Sag.

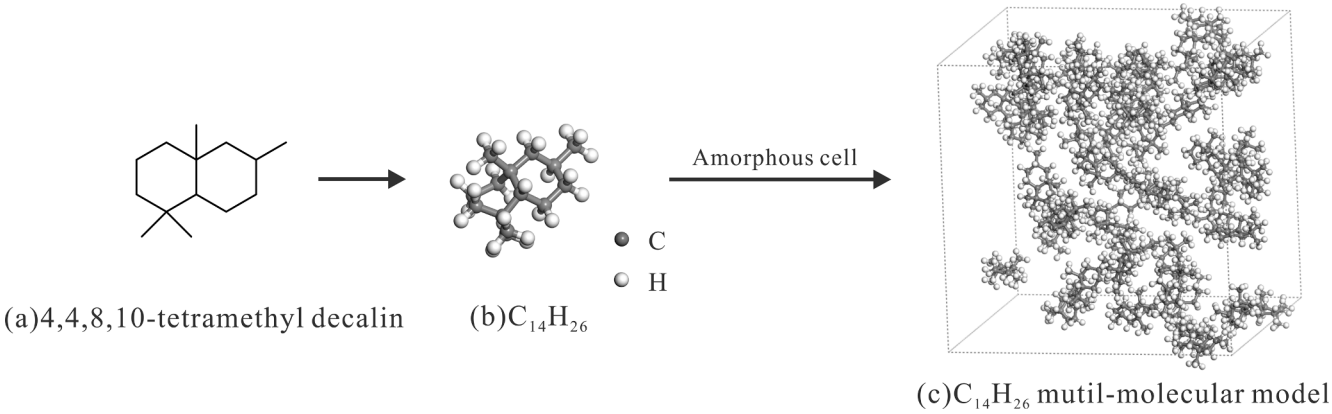

Fig. 2. Molecular model of 4,4,8,10-tetramethyl decalin ($C_{14}H_{26}$).

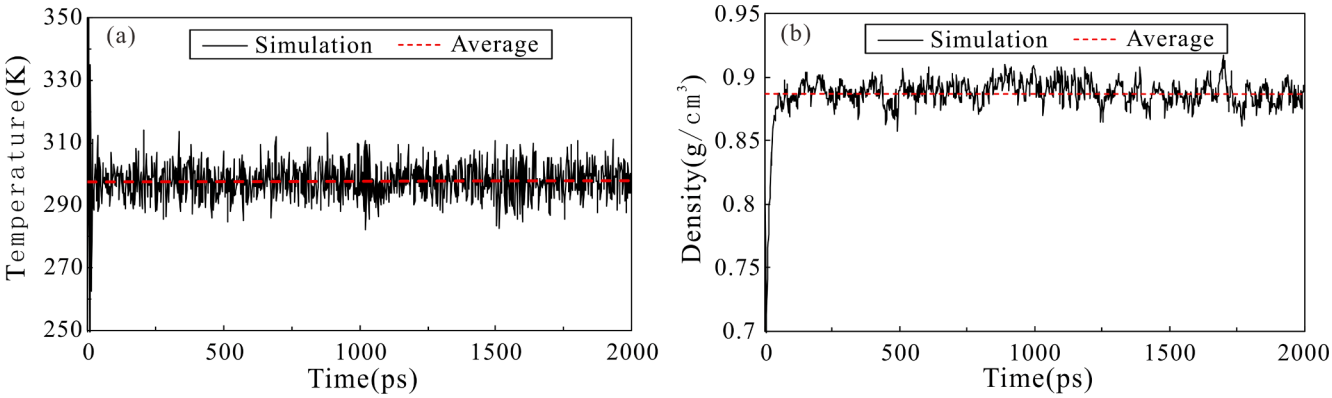

Fig. 3. Equilibrium of temperature(a) and density(b) of 4,4,8,10-tetramethyl decalin cell.

2.3. Bond dissociation energy calculations

The bond dissociation energy (*De*) of the main initial reactions observed during the ReaxFF MD simulation was determined using the Gaussian 09 program through the Density Functional Theory (DFT) method. For the DFT calculation, the first step involved geometrical optimization, where the most stable molecular structures of the reactants and products were obtained. Subsequently, vibration frequency analyses were conducted to evaluate the vibrational modes of the optimized structures. All geometrical optimization and vibration frequency analyses were performed at M062X method with the 6–311++G(d,p) basis set[34–36]. The def2TZVP basis set was applied in single point energy calculation [35]. By comparing the total energies of the reactant and product states, the bond dissociation energies were accurately calculated. The utilization of DFT and the selected basis set allowed for reliable determination of the bond dissociation energies, providing valuable insights into the stability and reactivity of the studied molecular systems. According to the reaction of $AB \rightarrow A\cdot + B\cdot$, *De* can be defined as,

$$De(AB) = E_{A\cdot} + E_{B\cdot} - E_{AB} \tag{2.1}$$

where $E_{A\cdot}$ and $E_{B\cdot}$ represent the total energy of the radical species $A\cdot$ and $B\cdot$ formed after breaking the chemical bond, respectively. E_{AB} is the total energy of the intact molecule with the chemical bond between A and B intact.

3. Results and discussion

3.1. Effect of temperature on the pyrolysis products of 4,4,8,10-tetramethyl decalin

To reveal the impact of temperature on the reactions and products of 4,4,8,10-tetramethyl decalin, a series of ReaxFF MD simulations were conducted within a temperature range of 2000 to 3000 K, with increments of 250 K. The changes in the number of fragments and main products were plotted in Fig. 4 to illustrate the simulation outcomes.

As shown in Fig. 4(a), the total number of fragments displays a sharp increase with rising simulation temperature, stabilizing at 3000 K. At lower temperatures, the number of ethylene (C_2H_4) molecules shows continuous growth, followed by a marked decline starting from 2750 K (Fig. 4(b)). Under the higher simulation temperature of 2750 K and 3000 K, the maximum number of C_2H_4 is achieved around 310 ps and 130 ps, respectively, with an approximate time difference of 180 ps. Notably, methane (CH_4) emerges as the predominant product during pyrolysis. Fig. 4(c) shows the progressive rise of CH_4, reaching peak values of 70 and 75 at simulated temperatures of 2750 K and 3000 K, respectively, indicating equilibrium in CH_4 production. The number of hydrogen (H_2) increases sluggishly at the beginning of pyrolysis, as depicted in Fig. 4(d). As the higher simulated temperature of 3000 K, the number of H_2 experiences a pronounced acceleration, culminating in its maximum value. In light of the fragment and product variations, it is evident that higher temperatures expedite the pyrolysis process of 4,4,8,10-tetramethyl decalin.

The variations in reactant and main species at different temperatures were analyzed in Fig. 5. The pyrolysis of 4,4,8,10-tetramethyl decalin primarily occurs between 2250 K and 3000 K, attributable to the significant fragment generation observed around 2000 K after approximately 90 ps in Fig. 4(a). Illustrated in Fig. 5, when simulating at 2250 K, the decomposition rate of 4,4,8,10-tetramethyl decalin was slow, with only one reactant molecule remaining after the 500 ps simulation. At 2500 K, the complete and rapid decomposition of 4,4,8,10-tetramethyl decalin occurred within about 165 ps. As the temperature rises to 2750 K and 3000 K, the consumption of 4,4,8,10-tetramethyl decalin initiates at around 91 ps and 27.3 ps, respectively.

Within the temperature range of 2250 K to 2500 K, the generation of ethylene (C_2H_4) shows the highest proportion and the fastest production rate due to its pronounced temperature dependence in ethylene production [15]. The number of propylene (C_3H_6), the third most abundant product, consistently increases from 2250 K to 2500 K. Nevertheless, in the temperature span of 2750 K to 3000 K, CH_4 gradually becomes the predominant product, while the abundance of C_2H_4 and C_3H_6 begins to decrease. The number of ethane (C_2H_6) and hydrogen gas (H_2) exhibit a continuous upward trend, surpassing C_3H_6 at 3000 K. This phenomenon infers that at higher simulated temperatures, further pyrolysis of olefins leads to the formation of alkanes and hydrogen, aligning with our previous research on *n*-tetradecane pyrolysis [16].

3.2. The mechanism of thermal cracking for 4,4,8,10-tetramethyl decalin

The process of oil cracking is intricate and dynamic, involving numerous chemical reactions and diverse intermediates [37,38]. Reaxff–MD simulation provides a practical approach to capturing

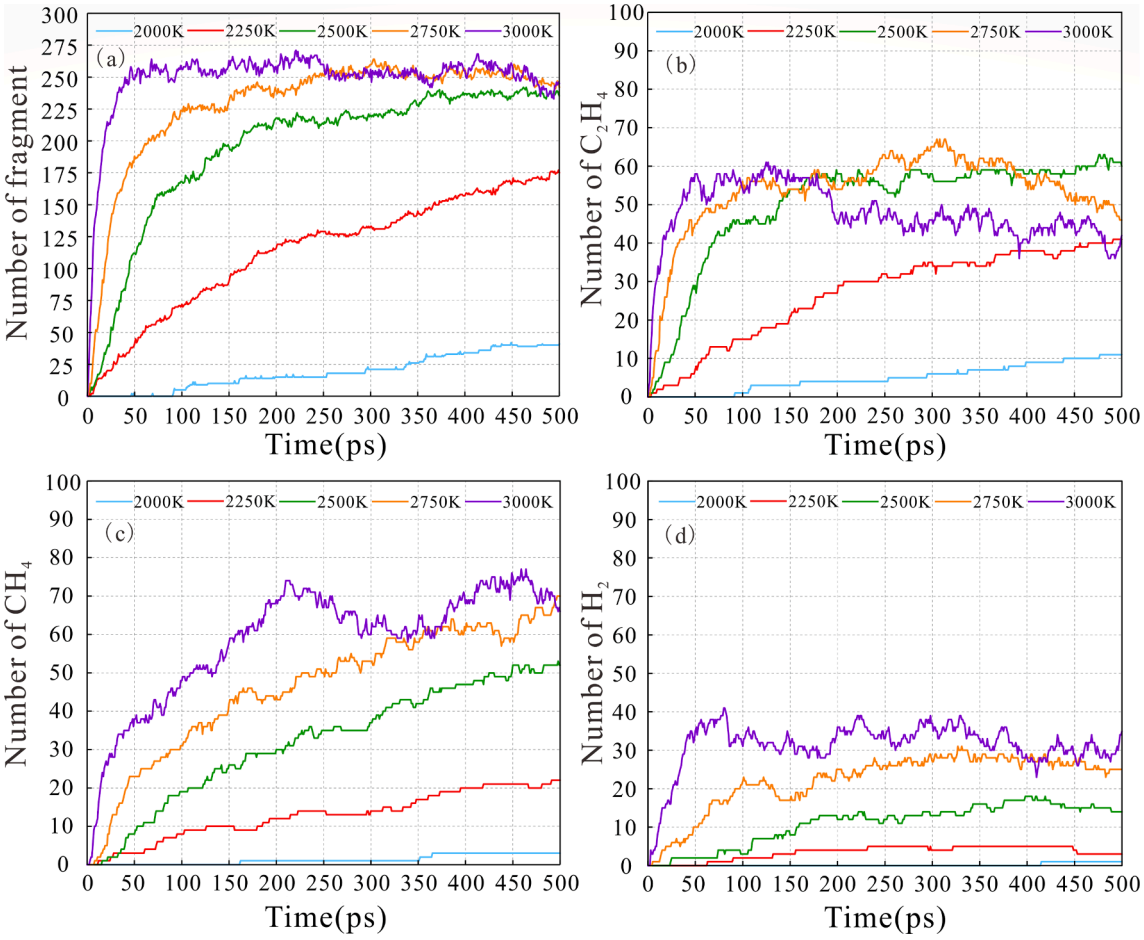

Fig. 4. The number of (a) total fragments, (b) ethylene, (c) methane, and (d) hydrogen with simulation time during 4,4,8,10-tetramethyl decalin ReaxFF-MD pyrolysis under different simulation temperatures.

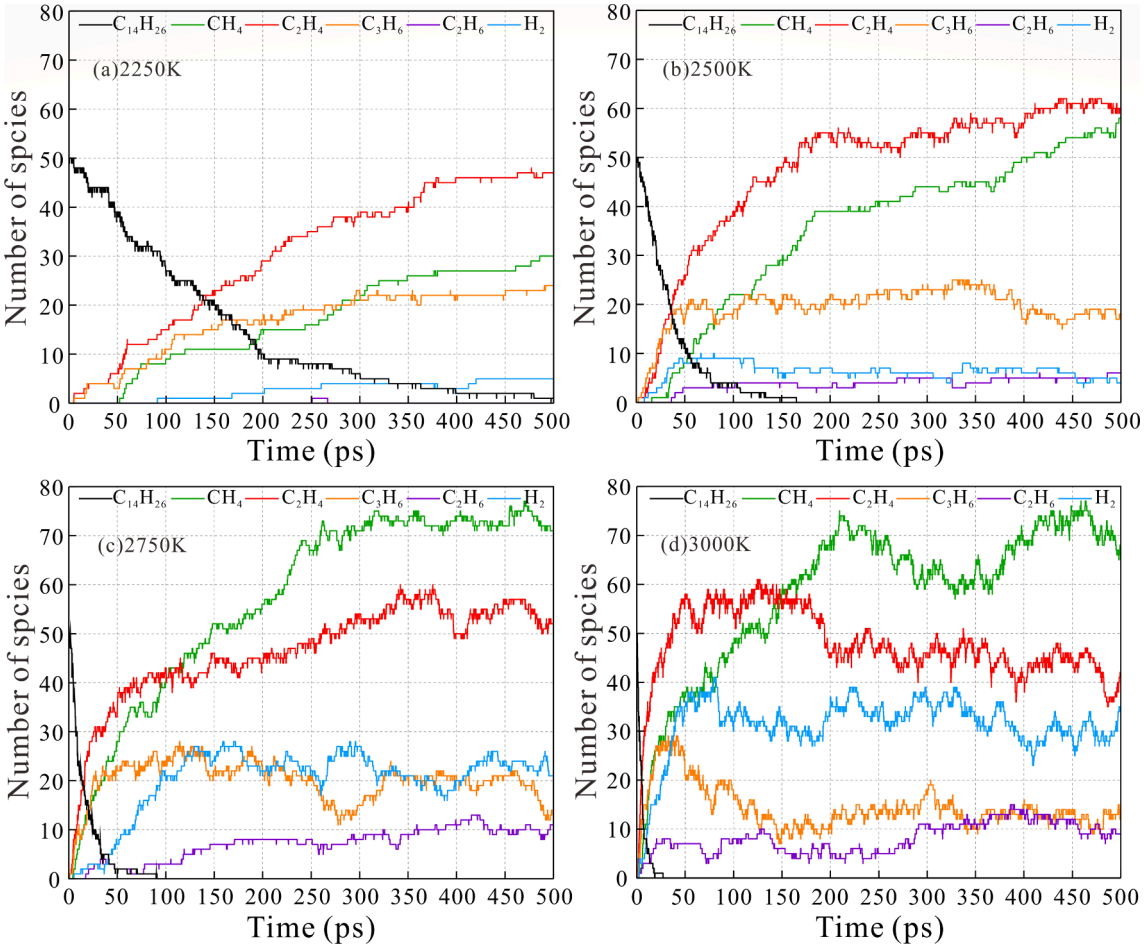

Fig. 5. The distributions of main pyrolysis products of 4,4,8,10-tetramethyl decalin with simulation time at different simulation temperatures: (a) 2250 K, (b) 2500 K, (c) 2750 K, and (d) 3000 K.

hydrocarbon cracking products at the corresponding simulation time. Intermediates and end products play a crucial role in dissecting the thermal cracking mechanism.

As shown in Fig. 6, the number of main initial pyrolysis products of 4,4,8,10-tetramethyl decalin within the temperature range of 2000 K to 3000 K. An examination of intermediates per picosecond reveals the frequent presence of C_8H_{13}, C_9H_{15}, and $C_{13}H_{23}$ free radicals, arising from the decomposition of 4,4,8,10-tetramethyl decalin. It can be seen that the initial pyrolysis process of 4,4,8,10-tetramethyl decalin leads to the formation of these ring–structured free radicals. The abstraction of a hydrogen atom from other molecules by these radicals is possible [48]. Considering the inherent instability of these free radicals and their propensity to rapidly engage with other molecules or atoms, the corresponding saturated molecules–specifically, C_8H_{14}, C_9H_{16}, and $C_{13}H_{24}$–have also been quantified.

As depicted in Fig. 6, the succession of free radicals and their corresponding saturated molecules resulting from the cracking of 4,4,8,10-tetramethyl decalin follows the sequence of C_{13} (the number of carbon atoms in the product is 13), C_9 (the number of carbon atoms in the product is 9), and C_8 (the number of carbon atoms in the product is 8) components, respectively.

Notably, this phenomenon was most prominently observed during the simulation at 2000 K. The initial species observed are $C_{13}H_{23}$ and $C_{13}H_{24}$, detected before 70 ps. Subsequently, at 72.6 ps, the presence of C_9H_{15} and C_9H_{16} was detected, succeeded by the appearance of other significant initiation species, C_8H_{13} and C_8H_{14}, at around 112.4 ps. This outcome implies that the formation of the $C_{13}H_{23}$ free radical via demethylation reaction transpires more rapidly than ring-opening reactions. As the simulation progresses, the number of C_9H_{15} plus C_9H_{16} and C_8H_{13} plus C_8H_{14} gradually surpasses that of $C_{13}H_{23}$ plus $C_{13}H_{24}$, indicating an enhanced proportion of ring-opening reactions during the initial decomposition of the reactant.

Importantly, higher temperatures significantly expedite the three types of reactions inherent in the initial pyrolysis process, especially at 3000 K. To comprehensively grasp the mechanism underlying the initial thermal cracking of 4,4,8,10-tetramethyl decalin, a series of analyses were conducted at 2000 K. This temperature range marks the initial phase of thermal cracking reactions.

As depicted in Fig. 7, an abundance of $C_{12}H_{22}$, $C_{11}H_{20}$, and $C_{11}H_{19}$ molecules becomes apparent after 60 ps. This observation can likely be attributed to the instantaneous production resulting from the prompt decomposition of $C_{13}H_{23}$ through demethylation reactions occurring at picosecond timescales [40,41]. This inference gains support from the fact that only these specific molecules, along with the corresponding amount of 4,4,8,10-tetramethyl decalin decomposition, were detected during this picosecond interval, alongside a limited production of olefins. The appearance of C_7H_{12} and C_7H_{11} signifies the immediate production of C_8H_{13} via the demethylation reaction. However, the absence of similar demethylation products for C_9H_{15} may be attributed to the challenge of distinguishing tertiary carbon atoms. Consequently, $C_{12}H_{22}$, $C_{11}H_{20}$, and $C_{11}H_{19}$ are considered intermediates involving C_{13}, while C_7H_{11} and C_7H_{12} are recognized as C_8 intermediates for the subsequent analysis.

The initial species formed during the pyrolysis of 4,4,8,10-tetramethyldecalin at 2000 K are illustrated in Fig. 8. The behavior of C_{13} and C_1 (the number of carbon atoms in the product is 1) intermediates

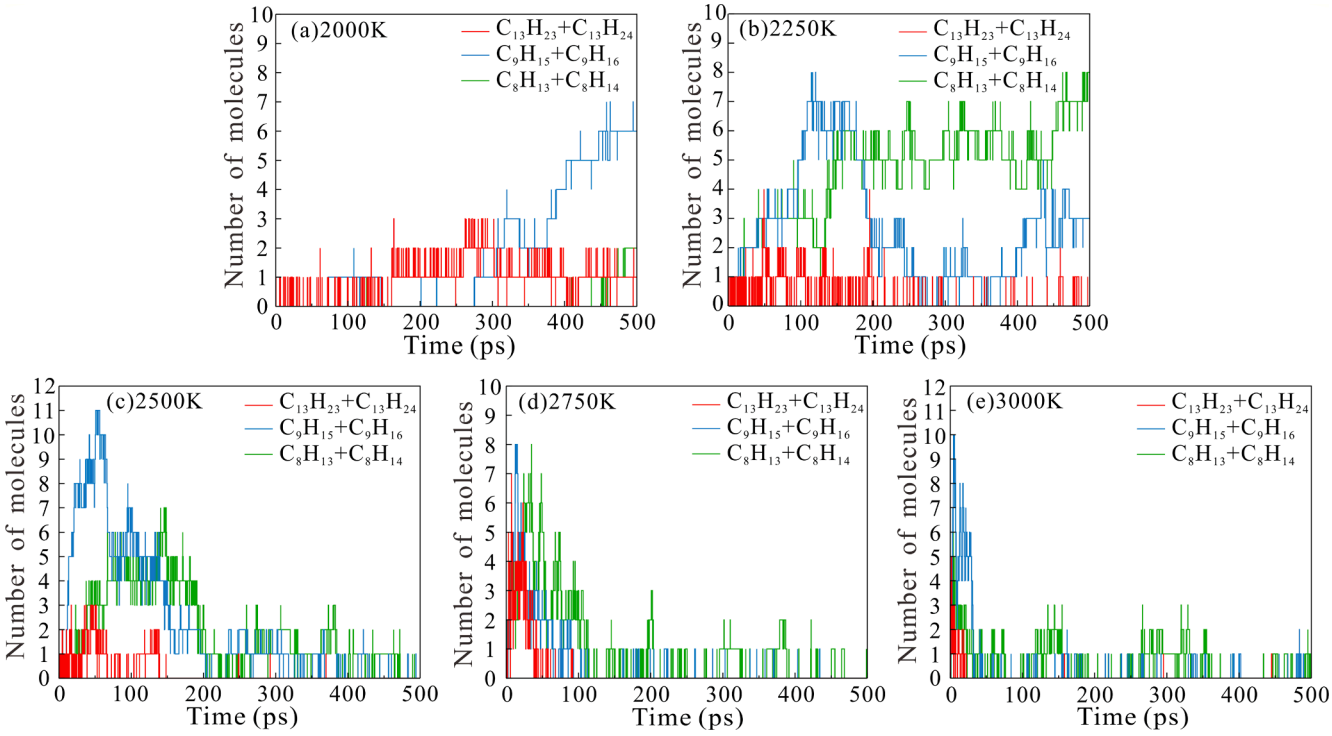

Fig. 6. The main initial pyrolysis products of 4,4,8,10-tetramethyl decalin at (a)2000 K, (b)2250 K, (c)2500 K, (d)2750 K and (e)3000 K simulated temperature.

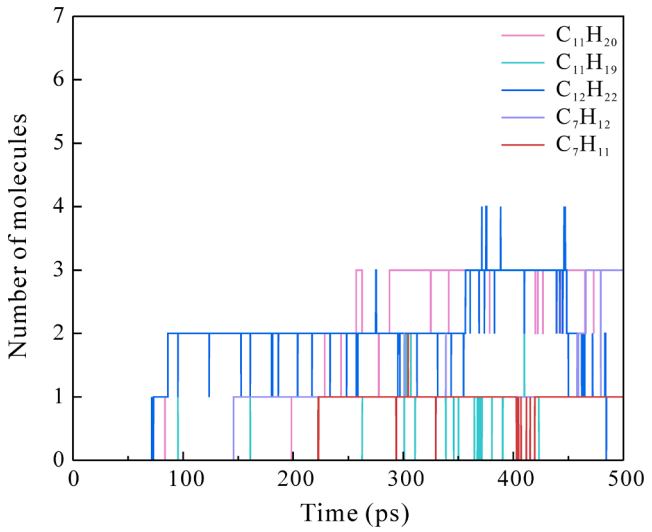

Fig. 7. The number of instantaneous productions from initial products by demethylation reaction at the temperature of 2000 K.

exhibits a consistent pattern up to 200 ps. Moreover, the accumulation of C_{13} intermediates closely corresponds to the generation of their respective intermediates. Due to the highly reactive chemical properties compared to cyclic hydrocarbons, chain-structured molecules or free radicals (such as C_6 (the number of carbon atoms in the product is 6) and C_5 (the number of carbon atoms in the product is 5) intermediates) are difficult to detect in the reactions occurring concurrently within picoseconds. Although the number of C_5 and C_6 intermediates is obviously lower than that of corresponding C_9 and C_8 intermediates, their numbers sustain a steady growth trend. These findings confirm that the thermal cracking process of 4,4,8,10-tetramethyl decalin yields C_{13}, C_9, and C_8 intermediates, along with their respective products.

The molecular masses of $C_{13}H_{23}$, C_9H_{15}, C_8H_{13} are 179, 123 and 109, respectively, which aligns with the crucial mass spectral fragments previously employed for identifying 4,4,8,10-tetramethyl decalin [4,5,39]. Previous research has indicated that organic molecules undergo ionization followed by fragmentation, yielding a distinct pattern of ions known as a mass spectrum [42]. The resemblance between this fragmentation pattern and the thermal cracking pattern has led to its application in investigating reaction pathways of organic compounds [43–45].

In this study, the mass spectrum of 4,4,8,10-tetramethyl decalin has a molecular ion at M^{+}·194, and a base peak ion at *m/z* 179, with diagnostic fragment ions at *m/z* 123, 109, 85, and 71, as shown in Fig. 9(a). In Fig. 9(b), at a simulation temperature of 2000 K, the relative frequency of intermediates follows a similar trend to the mass spectrum's ion peak abundances of 4,4,8,10-tetramethyl decalin. The result uncovers three pathways in the initial thermal pyrolysis of 4,4,8,10-tetramethyl decalin. The distribution of *m/z* 179 shows a predominant proportion, followed by *m/z* 123 and 109. Coupled with our prior statistical analysis of simulation trajectories in this study, it becomes apparent that demethylation reactions constitute the predominant portion of initiation reactions in the pyrolysis of 4,4,8,10-tetramethyl decalin. The remaining two mechanisms of initial pyrolysis involve the cleavage of C–C bonds within the ring to form a cycloalkyl group, as well as the generation of corresponding unstable chain radicals with extremely short lifespans.

After gaining a comprehensive understanding of the thermal cracking mechanisms of 4,4,8,10-tetramethyl decalin by analyzing the initial pyrolysis products, a series of DFT simulations were performed to calculate the bond dissociation energies of the initial reactions, specifically the bond dissociation enthalpies, as evidence to verify the three pyrolysis pathways above.

Fig. 10 shows 5 initial reaction pathways of 4,4,8,10-tetramethyl decalin pyrolysis. Paths 1–3 are classified as the demethylation reaction. Paths 4–5 are classified as the ring–opening reaction. Pathway 3 is the main pathway for the initiation reaction, the bond dissociation energy of path 3 is the lowest (304.35 kJ/mol). Followed by pathways 1–2, the bond dissociation energies of these reactions are much higher than that of pathway 3, which are 334.85 and 342.07 kJ/mol, respectively.

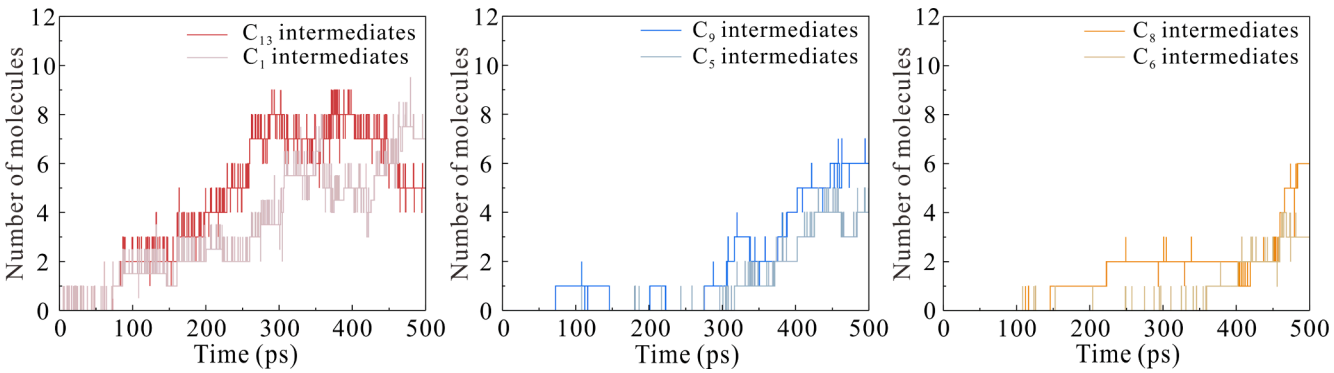

Fig. 8. The main initial intermediates generated by of 4,4,8,10-tetramethyl decalin at 2000 K simulated temperature.

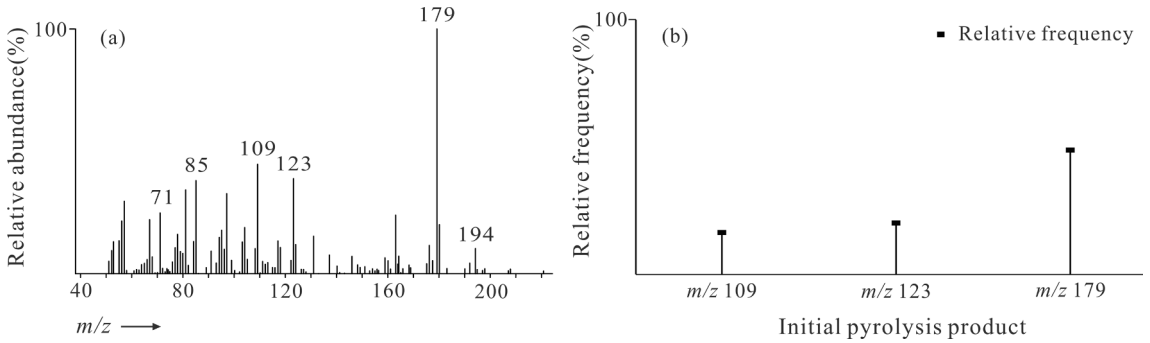

Fig. 9. The comparison of (b)the total number of each initial pyrolysis product at maximum at 2000 K with (a)the mass spectra. In Fig. 13(b), *m/z* 109 represents C_8 intermediates, *m/z* 123 represents C_9 intermediates, *m/z* 179 represents C_{13} intermediates.

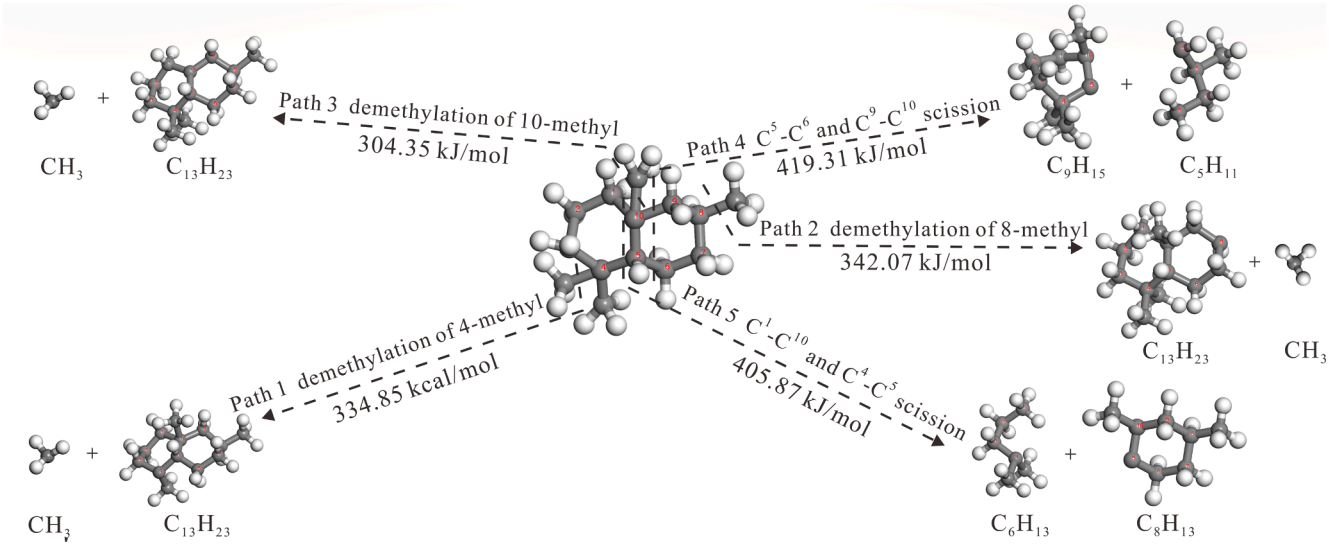

Fig. 10. Main initial reactions of 4,4,8,10-tetramethyl decalin observed in the ReaxFF–MD simulation.

For ring–opening reactions, the bond dissociation energies of pathways 4–5 are 419.31 and 405.87 kJ/mol, respectively. The bond dissociation energies for different reactions increase in the order path 3 < path 1 < path 2 < path 5 < path 4. Therefore, the apparent predominance of the number of *m/z* 179 compounds is well explained in Fig. 10. The similar bond dissociation energies of pathway 4–5 correlate well with the relative frequency between *m/z* 123 and 109 in Fig. 9. Meanwhile, the result serves as evidence for C_9 and C_8 intermediates with the corresponding products are difficult to detect in the initial reactions, which is consistent with the previous analysis results in Figs. 6 and 8.

3.3. Effect of molecular structure on pyrolysis of C_{14} hydrocarbon

3.3.1. Effect of molecular structure on pyrolysis rate

Time evolution of 4,4,8,10-tetramethyl decalin ($C_{14}H_{26}$) and *n*-tetradecane ($C_{14}H_{30}$) in the first 200 ps at the temperature range of 2000 K to 3000 K is shown in Fig. 11. As the temperature rises, the decomposition rate of $C_{14}H_{26}$ and $C_{14}H_{30}$ are significantly accelerated. At 2000 K, the number of $C_{14}H_{26}$ decreases to around 43 molecules, while the remaining $C_{14}H_{30}$ molecules amount to 44. With the temperature further increasing to 2250 K, the number of $C_{14}H_{26}$ molecules is 5 less than that

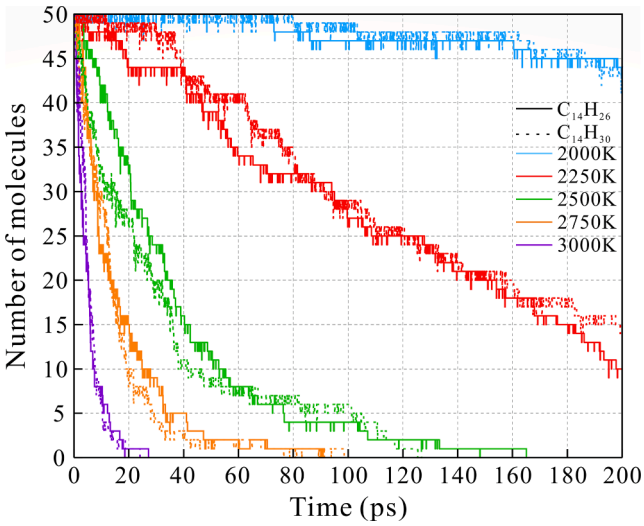

Fig. 11. Decomposition of 4,4,8,10-tetramethyl decalin and *n*-tetradecane in the first 200 ps under different temperatures.

of $C_{14}H_{30}$ at 200 ps. This finding indicates a considerably faster pyrolysis rate for $C_{14}H_{26}$ compared to $C_{14}H_{30}$. The observation aligns with previous research suggesting that the pyrolysis rate of cycloalkane is notably swifter than that of straight-chain hydrocarbons with an equivalent number of carbon atoms [13]. However, the pyrolysis rates of $C_{14}H_{26}$ and $C_{14}H_{30}$ exhibit minimal disparity over a higher temperature range of 2500 K to 3000 K, which indicates that the influence of molecular structure predominates during the initial stage of hydrocarbon cracking.

The decomposition time at various simulation temperature of 4,4,8,10-tetramethyl decalin is shown in Fig. 12. At the simulation temperature of 2000 K and 2250 K, the disintegration of 4,4,8,10-tetramethyl decalin respectively takes place around 72.1 ps and 4.7 ps, then consecutively proceeds in the following 427.9 ps and 495.3 ps. Between 2500 K and 3000 K, the initial pyrolysis of 4,4,8,10-tetramethyl decalin molecules occurred at 1.8 ps, 0.5 ps and 0.3 ps, and the completed pyrolysis of all 4,4,8,10-tetramethyl decalin molecules was observed at 165.2, 90.5 and 27.3 ps, respectively. After the initial decomposition reaction, the rest molecules generated from the initial reactions crack further into new products in the following simulation time. The pyrolysis process of 4,4,8,10-tetramethyl decalin can be divided into three stages determined by the decomposition time on the investigation of *n*-tetradecane by Li et al. [16]. As shown in Table 1, the initial decomposition of 4,4,8,10-tetramethyl decalin occurs at 72.1 ps, which is 7.8 ps earlier than that of *n*-tetradecane at 2000 K. At the temperature of 2250 K, the initial pyrolysis of *n*-tetradecane takes place after the first 11.9 ps, which is 7.2 ps slower than that of 4,4,8,10-tetramethyl decalin. The results imply that the pyrolysis rate of 4,4,8,10-tetramethyl decalin is relatively faster compared to *n*-tetradecane at 2000 K and 2250 K.

3.3.2. *Effect of molecular structure on pyrolysis products*

The number of various products generated by 4,4,8,10-tetramethyl decalin and *n*-tetradecane pyrolysis under different temperatures at the end of 500 ps is shown in Fig. 13. The number of C_1 is the most abundant product in the decomposition of 4,4,8,10-tetramethyl decalin at 2000 K. Furthermore, the number of C_1 generated from 4,4,8,10-tetramethyl decalin is significantly higher than that of *n*-tetradecane at 2000 K. This result indicates that the cracking of 4,4,8,10-tetramethyl decalin is contributed to the formation of methane compared to *n*-tetradecane in the initial pyrolysis stage. According to the initial reactions of *n*-tetradecane observed in the Reaxff–MD simulation (Fig. 14), the bond dissociation energies of the demethylation reaction (Path 1) is 361.76 kJ/mol, which is 19.69 ~ 57.41 kJ/mol higher than that of 4,4,8,10-tetramethyl decalin. The results show that CH_3 free radicals will be generated more readily from 4,4,8,10-tetramethyl decalin, which leads to the formation of CH_4 in the following reactions. As the simulated temperature increased to 3000 K, *n*-tetradecane produced a greater amount of C_1 than 4,4,8,10-tetramethyl decalin.

The amount of C_2–C_5 (gaseous hydrocarbons) produced by *n*-tetradecane is significantly greater than that of 4,4,8,10-tetramethyl decalin in the entire simulation. Meanwhile, 4,4,8,10-tetramethyl decalin shows a remarkable advantage in producing C_6-C_{13} (liquid products) between 2000 K and 2500 K. The results indicate that straight-chain alkanes serve as the primary precursors for C_2–C_5 short-chain gaseous hydrocarbons, while the cracking of the bicyclic sesquiterpane predominantly contributes to the formation of C_6–C_{13} liquid hydrocarbons.

As shown in Fig. 13, the bond dissociation energy of pathway 5 is the lowest, followed by path 1, path 2, path 6, path 4, path 3, and path 7. Therefore, it can be seen that *n*-tetradecane prefers to form C_5H_{11} and C_9H_{19} radicals in the initial pyrolysis stage.

The number of methane, ethane and propane by 4,4,8,10-tetramethyl decalin and *n*-tetradecane are listed separately in Fig. 15(a) and to be separately analyzed. The pyrolysis of 4,4,8,10-tetramethyl decalin demonstrates a significant advantage over *n*-tetradecane in terms of methane formation within the temperature range from 2000 K to 2750 K. However, at a temperature of 3000 K, the production of CH_4 from *n*-tetradecane gradually exceeds that from tetramethyl decalin due to the limited availability of hydrogen provided by tetramethyl decalin molecules. The result is in good agreement with previous reports, indicating that the hydrogen balance plays a crucial role in regulating the overall methane production within a closed system lacking alternative sources of hydrogen [37,46].

The straight-chain alkane pyrolysis process generates more C_2H_6 and C_3H_8 molecules than that of the bicyclic sesquiterpene, especially in the early stage of pyrolysis at lower temperatures. This result infers that the pyrolysis pathway of cyclic hydrocarbons leading to the formation of C_2H_6 and C_3H_8 via successive cleavages of C–C bonds in the carbon ring is difficult to occur. For the tendency of C_3H_8 produced by *n*-tetradecane, it reaches the maximum value at 2250 K. Subsequently, C_3H_8 undergoes further decomposition into lower molecular weights hydrocarbons such as CH_4. By contrast, the number of C_3H_8 remain nearly constant between 2500 K and 3000 K in the pyrolysis of 4,4,8,10-tetramethyl decalin. This observation suggests that the decomposition of C_3H_8 to form CH_4 occurs earlier in the pyrolysis of the straight-chain alkane.

The yield of the main gaseous hydrocarbons such as CH_4, C_2H_6, and C_3H_8 generated in the gaseous hydrocarbons and the straight-chain alkane decomposition are shown in Fig. 15(b). At each simulation temperature, the yield of methane produced by 4,4,8,10-tetramethyl decalin is the highest among the gaseous hydrocarbons, even among the yield of *n*-tetradecane pyrolysis gaseous hydrocarbons. It can be seen that tetramethyl decalin is more favorable for methane formation. Between 2000 K and 2250 K, the yield of C_2H_6 and C_3H_8 generated from 4,4,8,10-tetramethyl decalin is negligible compared to that of *n*-tetradecane. However, the yields of ethane and propane obtained from both 4,4,8,10-tetramethyl decalin and *n*-tetradecane are nearly indistinguishable at 3000 K. This finding shows that the yield of ethane and propane is limited by molecular structure at the higher temperature.

3.4. *Kinetic analysis of 4,4,8,10-tetramethyl decalin pyrolysis*

The first–order kinetic analysis of the pyrolysis of 4,4,8,10-tetramethyl decalin is significant in elucidating the kinetic behavior and characteristics of bicyclic sesquiterpanes in crude oil. In this study, the number of 4,4,8,10-tetramethyl decalin molecules is used instead of the concentration. The consumption rate of 4,4,8,10-tetramethyl decalin is used to describe the first-order kinetics of the pyrolysis reaction of 4,4,8,10-tetramethyl decalin, i.e.

$$4,4,8,10\text{ - tetramethyl decalin} \xrightarrow{k} \text{product} \tag{3.1}$$

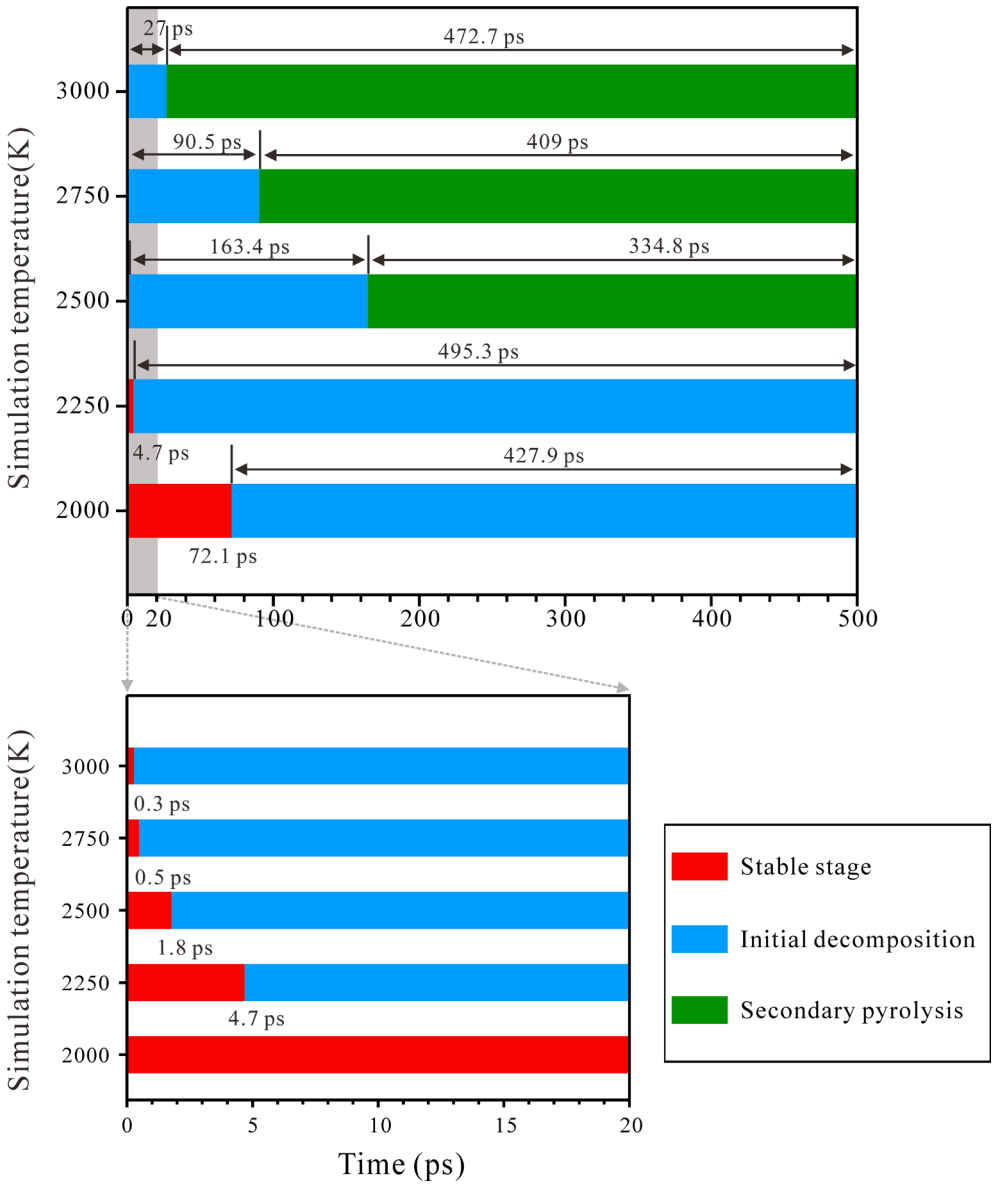

Fig. 12. Variations of decomposition time for 4,4,8,10-tetramethyl decalin ReaxFF-MD pyrolysis with the increase of simulation temperature.

Table 1
The decomposition time of 4,4,8,10-tetramethyl decalin and *n*-tetradecane in different pyrolysis stage.

	n-tetradecane			4,4,8,10-tetramethyl decalin		
	Stable stage	Initial decomposition	Secondary pyrolysis	Stable stage	Initial decomposition	Secondary pyrolysis
2000 K	79.9 ps	420.1 ps	/	72.1 ps	427.9 ps	/
2250 K	11.9 ps	385.7 ps	102.4 ps	4.7 ps	495.3	/
2500 K	0.4 ps	126.4 ps	373.2 ps	1.8 ps	163.4 ps	334.8 ps
2750 K	0.3 ps	98.3 ps	401.4 ps	0.5 ps	90.5 ps	409 ps
3000 K	0.2 ps	23.8 ps	475.9 ps	0.3 ps	27 ps	472.7

According to the variation of the number of 4,4,8,10-tetramethyl decalin molecules with time in the pyrolysis process at a range of 2000 K–3000 K, the initial reaction rate constants (k) of 4,4,8,10-tetramethyl decalin were calculated by linear fitting through the first–order rate law equation:

$$\ln N0 - \ln Nt = k(t - t0) \tag{3.2}$$

where N_0 is the number of 4,4,8,10-tetramethyl decalin molecules, t_0 is the time when pyrolysis starts, N_t is the number of 4,4,8,10-tetramethyl decalin molecules at the time of t. Then, the rate constant k of 2000 K–3000 K are put into the following expression of the Arrhenius equation to fit the relationship between the reaction rate and the temperature:

$$k = A\exp(-E_a/RT) \tag{3.3}$$

where A is the pre-exponential factor, E_a is the apparent activation energy, R is the gas constant and T is the thermodynamic temperature.

The Arrhenius fitting plot of the rate constants is shown in Fig. 16,

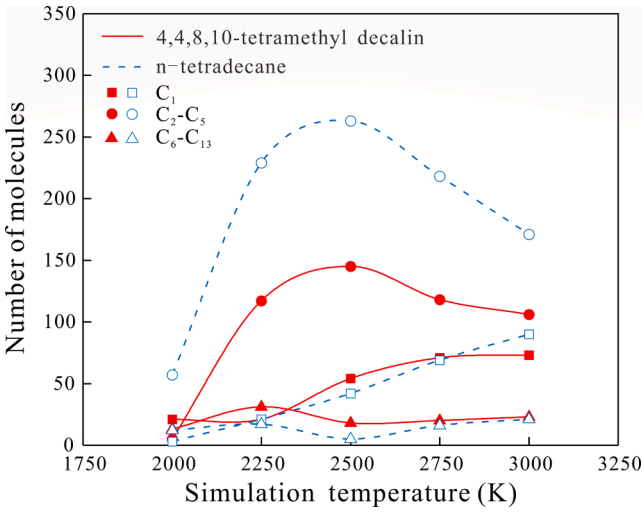

Fig. 13. Comparison of the number of various products generated by 4,4,8,10-tetramethyl decalin and *n*-tetradecane pyrolysis with the increasing simulation temperature.

from which the pre-exponential factor was calculated as $A = 1.18 \times 10^9$ s^{-1}, and the apparent activation energy of thermal decomposition as E_a = 227.09 kJ/mol (54.25 kcal/mol).

The pyrolysis apparent activation energy E_a for *n*-tetradecane obtained by ReaxFF–MD simulation is 235.35 kJ/mol (56.22 kcal/mol) in the previous study [16], which is higher than that of 4,4,8,10-tetramethyl decalin. The results indicate that 4,4,8,10-tetramethyl decalin in crude oil preferentially cracks than the normal C_{14} alkane counterpart, which is also consistent with the comparison of decomposition rate shown in Fig. 11. In addition, the previous studies on the kinetics of hydrocarbons with different molecular structure and the same number of carbon atoms show that the decomposition rate of cycloalkane is faster than that of their normal alkane counterparts. For example, Xin et al. [13] reported that the activation energy of cyclopentane decomposition is 201.56 kJ/mol, which is lower than that of *n*-pentane decomposition (228.33 kJ/mol). The report shows that the decomposition of cyclopentane has a higher pyrolysis rate than *n*-pentane.

3.5. Insights for subsurface oil cracking

Cracking process of crude oil under geological conditions is very complex [37,38]. The pyrolysis products of various components of crude oil have different contributions to the formation of oil and natural gas reservoirs. As a frequently detected bicyclic sesquiterpanes with 14 carbon atoms in crude oil, 4,4,8,10-tetramethyl decalin is selected to investigate the behaviors and characteristics of naphthenic hydrocarbon in crude oil thermal cracking process at different geological thermal evolution stages. As a typical normal alkane, the *n*-tetradecane in the previous study is also discussed here for comparison.

According to the composition of products under different temperatures, the thermal cracking process of 4,4,8,10-tetramethyl decalin can be also divided into thermal stability stage (2000 K–2250 K), primary formation of gases from liquid oil (2250 K–2750 K), and secondary alternation of primary gas to dry gas stage (>2750 K), corresponding to the subsurface and laboratory thermal evolution stages of crude oil (Table 2).

The number of methane is relatively lower at a temperature lower than 2250 K, and it remains stable increasing at maturation levels of primary and secondary stages (Fig. 13). The 4,4,8,10-tetramethyl decalin produced relatively more methane than normal tetradecane under same temperature (≤2750 K), which may be attributed to more methyl group on the cycloparaffin. However, the number of methane for 4,4,8,10-tetramethyl decalin keeps overall constant and is lower than that of normal tetradecane when the temperature is higher than 2750 K (Fig. 13). Methane is no longer produced during the high maturation stage, which is mainly due to the relatively fewer hydrogen atoms for 4,4,8,10-tetramethyl decalin molecules.

C_2–C_5 molecules begin to yield from 2000 K and get to their maximum at 2500 K, corresponding to the Ro of 2.0 % [47] for both normal tetradecane and 4,4,8,10-tetramethyl decalin. And then the number of reactant molecules continues to fall. This indicates that the C_2–C_5 compounds begin to crack to methane during the high maturity stage, which corresponds to the dry gas formation stage under geological conditions. In addition, the number of C_2–C_5 compounds for normal tetradecane is significantly higher than that of 4,4,8,10-tetramethyl (Fig. 13) because the ring-open reaction is likely to occur through the cleavage of more than two C–C bonds with higher bond dissociation energies, resulting in the formation of C_2–C_5 compounds. Correspondingly, the number of C_6–C_{13} for 4,4,8,10-tetramethyl decalin is relatively higher than that of normal tetradecane.

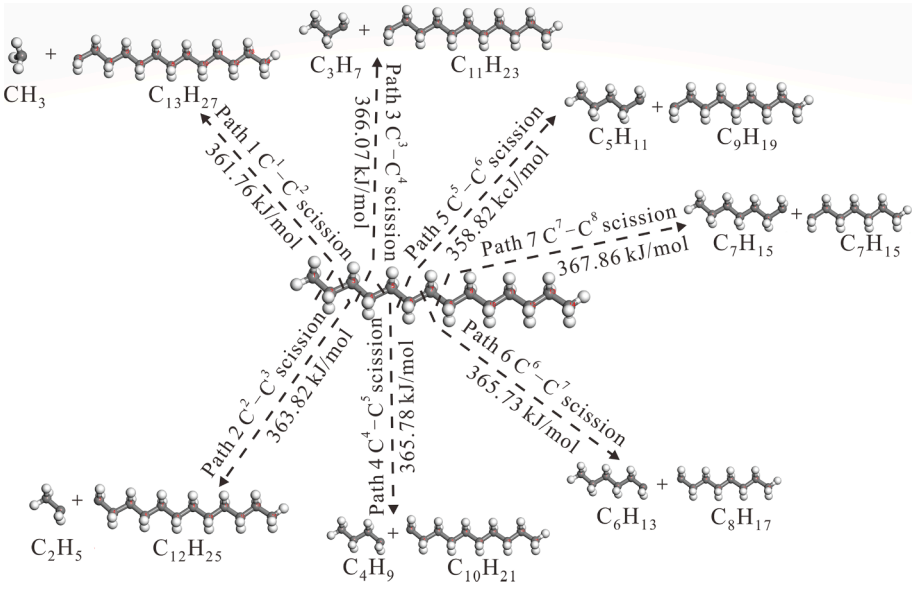

Fig. 14. Main initial reactions of *n*-tetradecane observed in the ReaxFF–MD simulation.

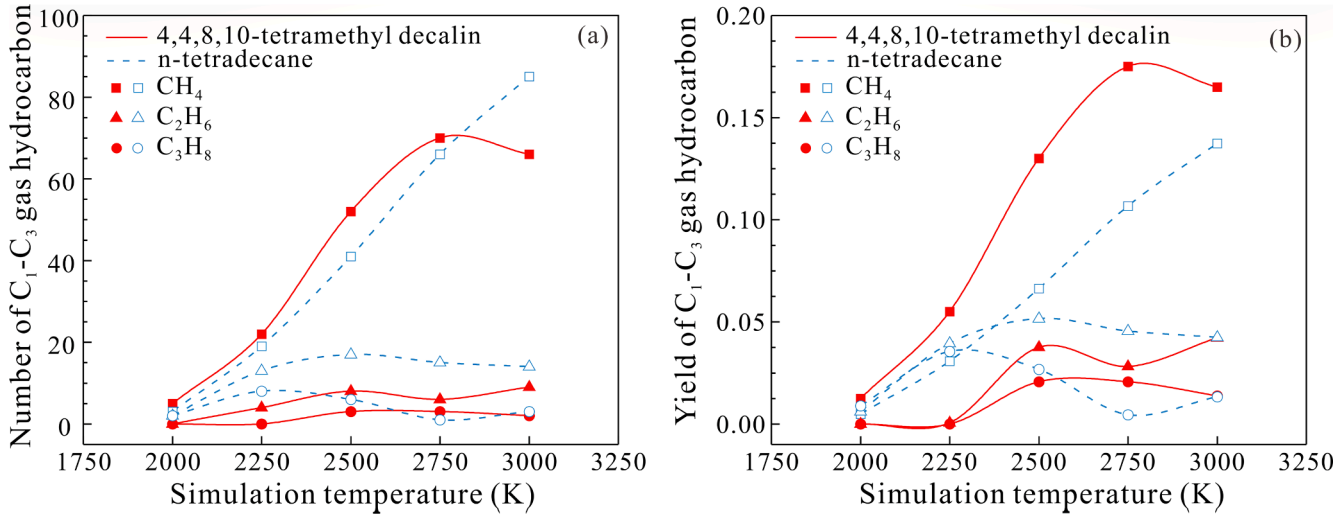

Fig. 15. Comparison of the numbers (a) and yields (b) of gaseous hydrocarbons (CH_4, C_2H_6, and C_3H_8) generated by 4,4,8,10-tetramethyl decalin and *n*-tetradecane pyrolysis.

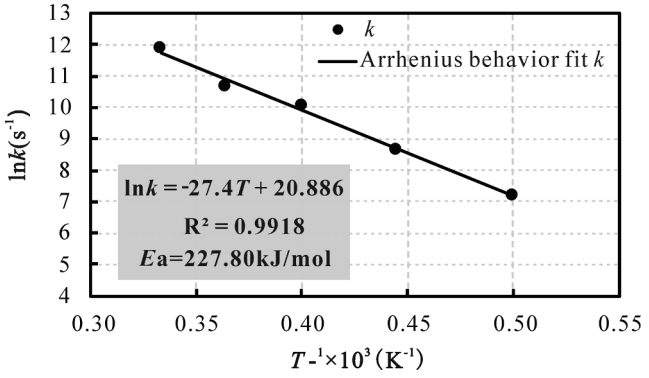

Fig. 16. Arrhenius plot with the fitted natural logarithm of rate constants (*k*) versus the inverse of temperature (*T*). Temperature range: 2000–3000 K. Linear fit equations with $R^2 = 0.9918$.

Table 2
Correspondence of molecular simulation temperature to Easy %Ro values in the geological evolution of oil cracking to gas.

Stage	Thermal stability	Primary formation of gases from liquid oil		Secondary alternation of primary gases to dry gas stage	Ref.
		Light oil stage	Gas condensate or wet gas stage		
Easy %Ro (%)	<1.20	1.2–1.75	1.75–2.40	>2.40	[24]
T_{MD} (K)	<2000–2250	2250–2500	2500–2750	>2750	[16]

This highlights how even minor differences in molecular structure can have significant impacts on the chemical composition of oil and gas reservoirs. Additionally, the different composition of pyrolysis products between 4,4,8,10-tetramethyl decalin and *n*-tetradecane at various thermal maturation levels are likely to reveal distinct contributions from bicyclic sesquiterpanes and normal alkanes in the formation and conservation of crude oil in reservoirs. Overall, these precursors involved in crude oil and natural gas formation at various stages of thermal stability were understood to provide valuable insights into studying subsurface oil cracking under geological conditions.

4. Conclusion

This paper explores the cracking processes of 4,4,8,10-tetramethyl decalin and *n*-tetradecane through a combination of ReaxFF molecular dynamics simulation and DFT calculations. The effect of temperature on the pyrolysis products of 4,4,8,10-tetramethyl decalin is discussed. The initial reactions, the kinetic behavior, the effect of molecular structure on the thermal cracking rate and pyrolysis products for 4,4,8,10-tetramethyl decalin and *n*-tetradecane are analyzed at different temperatures range of 2000 K to 3000 K. The main conclusions are as follows:

(1) The main intermediates and products obtained by the pyrolysis of 4,4,8,10-tetramethyl decalin include CH_4, C_2H_6, C_2H_4, C_3H_6, and H_2. The formation of olefins reaches a peak at 2750 K and then decreases owing to secondary cracking. The number of alkanes and hydrogen continuously increases and reaches the equilibrium stage at 3000 K.
(2) The main intermediates in the initial pyrolysis of 4,4,8,10-tetramethyl decalin are identified as $C_{13}H_{23}$, C_9H_{15}, and C_8H_{13} free radicals. These free radicals share molecular characteristics with the structures of diagnostic fragment ions at 179, 123, and 109 in mass spectrometric analysis.
(3) The initial pyrolysis reactions of C_{14} hydrocarbons mainly occurred at the C–C bonds. Five main pyrolysis channels of 4,4,8,10-tetramethyl decalin are identified, involving reactions such as the formation of $C_{13}H_{23}$ and CH_3 radical through the loss of methyl radical, and the generation of C_9H_{15} and C_5H_{11} or C_8H_{13} and C_6H_{13} radical via ring-open reactions. For *n*-tetradecane, initial pyrolysis is dominated by the cleavage of C–C bonds within the carbon chain, except for the terminal C–C bond.
(4) Kinetic analysis reveals the apparent activation energies for pyrolysis of 4,4,8,10-tetramethyl decalin and *n*-tetradecane to be 227.09 and 235.35 kJ/mol, respectively. The thermal cracking rate of 4,4,8,10-tetramethyl decalin surpasses that of *n*-tetradecane during the initial pyrolysis stage.
(5) The amount of C_1 and C_6-C_{13} of 4,4,8,10-tetramethyl decalin between 2000 K and 2750 K is much higher than that of *n*-tetradecane. The generation of C_2–C_5 by *n*-tetradecane is significantly greater than 4,4,8,10-tetramethyl decalin at the simulation process.

(6) Bicyclic sesquiterpanes and normal alkanes exhibit distinct contributions to the formation of oil and natural gas reservoirs at different thermal evolution stages. In the pyrolysis of 4,4,8,10-tetramethyl decalin, three discernible stages are distinguished: thermal stability stage (2000 K–2250 K), primary formation of gases from liquid oil (2250 K–2750 K), and secondary alternation of primary gases (>2750 K). Normal tetradecane proves effective in generating wet gases at the initial formation stage of wet gases, while 4,4,8,10-tetramethyl decalin emerges as a favorable precursor for methane and liquid hydrocarbons during the initial formation stage of light oil.

CRediT authorship contribution statement

Haochen Chen: Writing – review & editing, Writing – original draft, Software, Methodology, Investigation, Formal analysis, Data curation. **Meijun Li:** Writing – review & editing, Supervision, Methodology, Conceptualization. **Xiaoqiang Liu:** Writing – review & editing, Validation, Software. **Qiuya Han:** Writing – review & editing, Methodology, Investigation. **Wenke Li:** Writing – review & editing, Validation, Conceptualization. **Siyuan Zhang:** Software, Investigation, Data curation.

Declaration of competing interest

The authors declare that they have no known competing financial interests or personal relationships that could have appeared to influence the work reported in this paper.

Data availability

Data will be made available on request.

Acknowledgements

This work was funded by the National Natural Science Foundation of China (Grant No.42173054), Natural Science Foundation of Sichuan Province (No.2022NSFSC0182), and partly supported by the 18th "Challenge Cup" Competition for National College Students Extracurricular Academic and Technical Works. The authors are grateful for the guide by the researchers from Research Institute of Petroleum Exploration & Development. All calculated results were supported by the Sichuan University of Science & Engineering High-Performance Computing Center for providing computational. The authors thank Dr Xianggui Xue and Yushi Wen from the Institute of Chemical Materials, China Academy of Engineering Physics (CAEP) for help with the LAMMPS code.

References

[1] Yan G, Xu YH, Liu Y, Tang PH, Bin LW. Evolution and organic geochemical significance of bicyclic sesquiterpanes in pyrolysis simulation experiments on immature organic-rich mudstone. Pet Sci 2019;16:502–12. https://doi.org/10.1007/s12182-019-0326-6.
[2] Luo BJ, Wang YX, Meng QX, Yang XH, Li XY, Chen N. The geochemical significance of bicyclic sesquiterpanes in oil, coal and sediments. Sci China Ser B 1990;4:419–30. In Chinese with English abstract.
[3] Xia YQ, Luo BJ. The study on formation and evolution of bicyclic sesquiterpane by means of pyrolysis. Acta Sedimentol Sin 1994;3:106–13. In Chinese with English abstract.
[4] Ji L, He C, Zhang M, Wu Y, Li X. Bicyclic alkanes in source rocks of the Triassic Yanchang Formation in the Ordos Basin and their inconsistency in oil-source correlation. Mar Pet Geol 2016;72:359–73. https://doi.org/10.1016/j.marpetgeo.2016.02.021.
[5] Alexander R, Kagi RI, Noble R, Volkman JK. Identification of some bicyclic alkanes in petroleum. Org Geochem 1984;6:63–72. https://doi.org/10.1016/0146-6380(84)90027-5.
[6] Fleck S, Michels R, Izart A, Elie M, Landais P. Palaeoenvironmental assessment of Westphalian fluvio-lacustrine deposits of Lorraine (France) using a combination of organic geochemistry and sedimentology. Int J Coal Geol 2001;48:65–88. https://doi.org/10.1016/S0166-5162(01)00048-9.
[7] Wang TG, Simoneit BRT. Tricyclic terpanes in Precambrian bituminous sandstone from the eastern Yanshan region. North China Chem Geol 1995;120:155–70. https://doi.org/10.1016/0009-2541(94)00113-M.
[8] Fan P, Philp RP, Li Z, Yu X, Ying G. Biomarker distributions in crude oils and source rocks from different sedimentary environments. Chem Geol 1991;93:61–78. https://doi.org/10.1016/0009-2541(91)90064-X.
[9] Waples DW. Time and Temperature in Petroieum Formation: Application of Lopatin's iMethod to Petroieum Exploration. Am Assoc Pet Geol Bull 1980;64:916–26.
[10] van Duin ACT, Dasgupta S, Lorant F, Goddard WA. ReaxFF: A reactive force field for hydrocarbons. J Phys Chem A 2001;105:9396–409. https://doi.org/10.1021/jp004368u.
[11] Ding JX, Zhang L, Zhang Y, Han KL. A Reactive Molecular Dynamics Study of n-Heptane Pyrolysis at High Temperature. J Phys Chem A 2013;117:3266–78. https://doi.org/10.1021/jp311498u.
[12] Liu Y, Ding J, Han KL. Molecular dynamics simulation of the high-temperature pyrolysis of methylcyclohexane. Fuel 2018;217:185–92. https://doi.org/10.1016/j.fuel.2017.12.055.
[13] Xin LY, Liu C, Liu Y, Huo EG, Li QB, Wang XR, et al. Thermal decomposition mechanism of some hydrocarbons by ReaxFF-based molecular dynamics and density functional theory study. Fuel 2020:275. https://doi.org/10.1016/j.fuel.2020.117885.
[14] Lele A, Kwon H, Ganeshan K, Xuan Y, van Duin ACT. ReaxFF molecular dynamics study on pyrolysis of bicyclic compounds for aviation fuel. Fuel 2021:297. https://doi.org/10.1016/j.fuel.2021.120724.
[15] Wang Y, Gong S, Wang H, Li L, Liu G. High-temperature pyrolysis of isoprenoid hydrocarbon p-menthane using ReaxFF molecular dynamics simulation. J Anal Appl Pyrolysis 2021:155. https://doi.org/10.1016/j.jaap.2021.105045.
[16] Li M, Han Q, Liu X, Xu J, Chen H, Ma Y. New insights into the pyrolysis of n-tetradecane using ReaxFF molecular dynamics simulations: Implications for understanding the thermal cracking of subsurface crude oil. Energy Explor Exploit 2023;41:44–61. https://doi.org/10.1177/01445987221131111.
[17] Salmon E, van Duin ACT, Lorant F, Marquaire PM, Goddard WA. Thermal decomposition process in algaenan of Botryococcus braunii race L. Part 2: Molecular dynamics simulations using the ReaxFF reactive force field. Org Geochem 2009;40:416–27. https://doi.org/10.1016/j.orggeochem.2008.08.012.
[18] Salmon E, van Duin ACT, Lorant F, Marquaire PM, Goddard WA. Early maturation processes in coal. Part 2: Reactive dynamics simulations using the ReaxFF reactive force field on Morwell Brown coal structures. Org Geochem 2009;40:1195–209. https://doi.org/10.1016/j.orggeochem.2009.09.001.
[19] Qian Y, Zhan JH, Lai D, Li M, Liu X, Xu G. Primary understanding of non-isothermal pyrolysis behavior for oil shale kerogen using reactive molecular dynamics simulation. Int J Hydrogen Energy 2016;41:12093–100. https://doi.org/10.1016/j.ijhydene.2016.05.106.
[20] Hong D, Guo X. Molecular dynamics simulations of Zhundong coal pyrolysis using reactive force field. Fuel 2017;210:58–66. https://doi.org/10.1016/j.fuel.2017.08.061.
[21] De WQ, Wang JB, Li JQ, Tan NX, Li XY. Reactive molecular dynamics simulation and chemical kinetic modeling of pyrolysis and combustion of n-dodecane. Combust Flame 2011;158:217–26. https://doi.org/10.1016/j.combustflame.2010.08.010.
[22] Chen Z, Sun W, Zhao L. High-Temperature and High-Pressure Pyrolysis of Hexadecane: Molecular Dynamic Simulation Based on Reactive Force Field (ReaxFF). J Phys Chem A 2017;121:2069–78. https://doi.org/10.1021/acs.jpca.6b12367.
[23] Li WJ, Yu S, Zhang L, Chen JF, Cao WG, Lan YH. ReaxFF molecular dynamics simulations of n-eicosane reaction mechanisms during pyrolysis and combustion. Int J Hydrogen Energy 2021;46:38854–70. https://doi.org/10.1016/j.ijhydene.2021.08.234.
[24] Tian H, Wang ZM, Xiao ZY, Li XQ, Xiao XM. Oil cracking to gases: Kinetic modeling and geological significance. Chin Sci Bull 2006;51:2763–70. https://doi.org/10.1007/s11434-006-2188-8.
[25] Tian H, Xiao XM, Yang LG, Xiao ZY, Guo LG, Shen JG, et al. Pyrolysis of oil at high temperatures: Gas potentials, chemical and carbon isotopic signatures. Chin Sci Bull 2009;54:1217–24. https://doi.org/10.1007/s11434-008-0590-0.
[26] Dai Y, Zhao W, Xie H, Guo Y, Fang W. Pyrolysis kinetics and mechanism of ethylcyclohexane. J Anal Appl Pyrolysis 2020:145. https://doi.org/10.1016/j.jaap.2019.104723.
[27] Liu Y, Zhong Z, Xu S. Pyrolysis mechanism of tetrahydrotricyclopentadiene by ReaxFF reactive molecular dynamics simulations. Comput Theor Chem 2022;1213. 10.1016/j.comptc.2022.113735.
[28] Lindgren EB, Monteiro JGS, dos Santos AR, Fleming FP, Barbosa AGH. Initiation mechanisms and kinetics of the combustion of cyclopentane and cyclopentene from ReaxFF molecular dynamics. Fuel 2021:303. https://doi.org/10.1016/j.fuel.2021.121205.
[29] Aktulga HM, Fogarty JC, Pandit SA, Grama AY. Parallel reactive molecular dynamics: Numerical methods and algorithmic techniques. Parallel Comput 2012;38:245–59. https://doi.org/10.1016/j.parco.2011.08.005.
[30] Chenoweth K, van Duin ACT, Goddard WA. ReaxFF reactive force field for molecular dynamics simulations of hydrocarbon oxidation. J Phys Chem A 2008;112:1040–53. https://doi.org/10.1021/jp709896w.
[31] Xue XG, Meng LY, Ma Y, Zhang CY. Molecular Reactive Force-Field Simulations on the Carbon Nanocavities from Methane Pyrolysis. J Phys Chem C 2017;121:7502–13. https://doi.org/10.1021/acs.jpcc.7b00294.
[32] Shi K, Chen J, Pang X, Jiang F, Hui S, Zhang S, et al. Average molecular structure model of shale kerogen: Experimental characterization, structural reconstruction,

and pyrolysis analysis. Fuel 2024;355:129474. https://doi.org/10.1016/J.FUEL.2023.129474.
[33] Wang K, Zhang H, Wang X, Fan W. Study on pyrolysis mechanism of coal in hydrogen-rich atmosphere based on reactive molecular dynamics simulation. Int J Hydrogen Energy 2023. https://doi.org/10.1016/J.IJHYDENE.2023.08.060.
[34] Zhao Y, Truhlar DG. The M06 suite of density functionals for main group thermochemistry, thermochemical kinetics, noncovalent interactions, excited states, and transition elements: Two new functionals and systematic testing of four M06-class functionals and 12 other functionals. Theor Chem Acc 2008;120:215–41. https://doi.org/10.1007/s00214-007-0310-x.
[35] Leng L, Yang L, Zu H, Yang J, Ai Z, Zhang W, et al. Insights into glycine pyrolysis mechanisms: Integrated experimental and molecular dynamics/DFT simulation studies. Fuel 2023;351. https://doi.org/10.1016/j.fuel.2023.128949.
[36] Liu W, Yu W, Wang N, Chen J, Shen A. Pyrolysis mechanism of R601a/R245fa mixture: A ReaxFF-MD and DFT study. Comput Theor Chem 2023;1227. https://doi.org/10.1016/j.comptc.2023.114244.
[37] Hill RJ, Tang YC, Kaplan IR. Insights into oil cracking based on laboratory experiments. Org Geochem 2003;34:1651–72. https://doi.org/10.1016/S0146-6380(03)00173-6.
[38] Dominé F, Dessort D, Brévart O. Towards a new method of geochemical kinetic modelling: implications for the stability of crude oils. Org Geochem 1998;28:597–612. https://doi.org/10.1016/S0146-6380(98)00030-8.
[39] Peters K, Walters C, Moldowan JM. Biomarkers and Isotopes in the Environment and Human History. The Biomarker Guide 2005;1.
[40] Raza Z, Naz K, Ahmad S. Expected values of molecular descriptors in random polyphenyl chains. Emerg Sci J 2022;6(151–65). https://doi.org/10.28991/ESJ-2022-06-01-012.
[41] Rachman S, Komariah L, Andalia W, Hadiah F, Ramayanti C. Taguchi Experiment Design for DES K2CO3-glycerol performance in RBDPO Transesterification. Emerg Sci J 2023;7(917–27). https://doi.org/10.28991/ESJ-2023-07-03-018.
[42] Hamming MC, Foster NG. Fragmentation reactions—key to interpretation of mass spectra. Interpretation of Mass Spectra of Organic Compounds 1972:217–389. https://doi.org/10.1016/B978-0-12-322150-6.50009-1.
[43] Wang Y, Cao XY, Shi JC, Li X, Liu YF, Xu YJ. Tracking the dynamics of epoxy triglycerides during thermal oxidation by liquid chromatography-mass spectrometry. Food Control 2023;146. https://doi.org/10.1016/j.foodcont.2022.109523.
[44] Fahmey MA, Zayed MA, Keshk YH. Comparative study on the fragmentation of some simple phenolic compounds using mass spectrometry and thermal analyses. Thermochim Acta 2001;366:183–8. https://doi.org/10.1016/S0040-6031(00)00724-3.
[45] Fathalinejad S, Taarning E, Christensen P, Christensen JH. Chemical composition analysis of carbohydrate fragmentation products. J Anal and Appl Pyrolysis 2021;156:105112. https://doi.org/10.1016/J.JAAP.2021.105112.
[46] Balasubramanian R, Abishek A, Gobinath S, Jaivignesh K. Alternative fuel: hydrogen and its thermodynamic behaviour. J Human, Earth, Future 2022;3(195–203). https://doi.org/10.28991/HEF-2022-03-02-05.
[47] Han Q, Li M, Liu X, Xiao H, Ren J, Guo C. A maturation scale for molecular simulation of kerogen thermal degradation. Org Geochem 2023;175. https://doi.org/10.1016/j.orggeochem.2022.10450.
[48] Eldridge DL, Turner AC, Bill M, Conrad ME, Stolper DA. Experi-mental determinations of carbon and hydrogen isotope fractionations and methane clumped isotope compositions associated with ethane pyrolysis from 550 to 600 °C. Geochim Cosmochim Acta 2023;355:235–65. https://doi.org/10.1016/j.gca.2023.06.006.